Title
Ordering of water in opals with different microstructures

Journal
European Journal of Mineralogy, 27(2)

ISSN
0935-1221

Authors
Eckert, J
Gourdon, O
Jacob, DE
et al.

Publication Date
2015-03-01

DOI
10.1127/ejm/2015/0027-2428

Peer reviewed

Eur. J. Mineral.
2015, **27**, 203–213
Published online 18 December 2014

Ordering of water in opals with different microstructures

JÜRGEN ECKERT[1,2], OLIVIER GOURDON[2], DORRIT E. JACOB[3], CAGLA MERAL[4,5], PAULO J.M. MONTEIRO[4], SVEN C. VOGEL[2], RICHARD WIRTH[6] and HANS-RUDOLF WENK[7,*]

[1] Department of Chemistry, University of South Florida, Tampa, Fl 33620, USA
[2] Los Alamos National Laboratory, LANSCE, Los Alamos, NM 87545, USA
[3] Department of Earth and Planetary Sciences, Macquarie University, North Ryde, NSW 2109, Australia
[4] Department of Civil and Environmental Engineering, University of California, Berkeley, CA 94720, USA
[5] Middle East Technical University, 06800 Ankara, Turkey
[6] GeoForschungsZentrum, 14473 Potsdam, Germany
[7] Department of Earth and Planetary Science, University of California, Berkeley, CA 94720, USA
*Corresponding author, e-mail: wenk@berkeley.edu

Abstract: Opal has long fascinated scientists. It is one of the few minerals with an amorphous structure, and yet, compared to silica glass, it is highly organized on the mesoscale. By means of inelastic neutron scattering (INS), we could document that in four samples of opal at low temperature an ice-like structure of water is present, with details depending on microstructural characteristics. While FTIR spectra for all samples are nearly identical and thus not very informative, INS shows clear differences, highlighting the significance of microstructures. Neutron diffraction at 100 K on one of the opal samples provides evidence for crystalline cubic ice.

Key-words: opal; water; TEM; inelastic neutron scattering; neutron diffraction; FTIR.

1. Introduction

Opals occur in vesicles and veins, and form by precipitation from silica solutions and gels (*e.g*. Gaillou *et al.*, 2008). In sedimentary cherts amorphous silica is often inherited from fossil fragments. During subsequent diagenesis, amorphous opal (opal A) converts to metastable cristobalite/tridymite (opal-CT) and finally to quartz (*e.g*. Kastner *et al.*, 1977; Lynne & Campbell, 2003).

Baier (1932) was the first to attribute the iridescent colors of opals to a periodic microstructure, but it was only later that electron microscope investigations confirmed a regular arrangement of close-packed spheres in precious opals (Jones *et al.*, 1964). Small-angle neutron scattering was used to quantify the range of sizes of the spherules that is related to their distinctive play of color (Graetsch & Ibel, 1997). A recent systematic study of the microstructure of different opal samples documented spheres linked by amorphous silica cement with nanoporosity (Gaillou *et al.*, 2008).

Some 500 minerals are known to incorporate water in various forms (Aines & Rossman, 1984). Water can be present as free, hydrogen-bonded water (*e.g*. in clays), as a ligand to a cation (*e.g*. in sheet silicates), or as a surface species (*e.g*. in zeolites). Frequently, the interaction of water with its surroundings is relatively weak (van der Waals or hydrogen-bonding interactions), with the result that water is structurally disordered, which makes it difficult to obtain structural information, even with methods that are sensitive to hydrogen or deuterium such as neutron diffraction.

Compared with other silica minerals and silica glass, opal contains a large amount of water (1–10 wt. %, Graetsch *et al.* 1994; Graetsch & Ibel, 1997). Infrared studies at ambient conditions indicate that water is present in various forms: free water between spheres, surface water, and silanol (Si-OH) groups on the surface of the silica spherules (Day & Jones, 2008; Bobon *et al.*, 2011). The presence of silanol groups in silica has been firmly established by nuclear magnetic resonance spectroscopy (Brown *et al.*, 2003). However, surface water, hydrogen-bonded to the layer of silanol groups covering the silica surface, represents only a small amount of the detected water. The structural state of the rest of the water is poorly known. The present study uses vibrational spectroscopy by inelastic neutron scattering (INS), and neutron powder diffraction to investigate the structure of water in four opal samples at a range of temperatures. It follows up on an earlier report of Sosnowska *et al.* (1997), taking advantage of improved experimental capabilities.

The vibrational spectra of water and ice are readily observed by inelastic neutron scattering (INS), particularly

DOI: 10.1127/ejm/2015/0027-2428
0935-1221/15/0027-2428 $ 4.95

at lower frequencies. The advantage of INS over FTIR for this purpose is based on the fundamental differences in the interaction of neutrons as opposed to photons with matter.

First, neutrons scatter from the atomic nuclei, which is essentially a point interaction, so that there are no symmetry-based selection rules in INS, unlike in optical spectroscopy. While such selection rules can be very useful in the interpretation of optical spectra, they are broken in ice because of local structural disorder, which in turn makes the spectral analysis complex (Li & Kolesnikov, 2002). IR and Raman spectroscopy are most sensitive to modes such as O-H stretching and bending, but less so to vibrations of H_2O molecules against each other (Li & Kolesnikov, 2002) or whole-body librations, where only small changes in polarisability or dipole moment are involved.

Second, incoherent neutron scattering cross sections for hydrogen are four orders of magnitude larger than those for most other nuclei ($\sigma_{inc} = 80.26$ barn for H, 0.004 barn for Si, and 0.0008 barn for O), which, in combination with large vibrational amplitudes, makes the observation of hydrogen dynamics (and, therefore, water) with INS rather direct, even in the presence of a large amount of host material such as silica. The whole-body translational and librational modes of water therefore typically have strong intensities in the INS vibrational spectrum because of the relatively large amplitude of motion of the hydrogen atoms in these modes, which in turn involve only small changes in the dipole moment that governs IR spectral intensities. The bending modes of silanol groups can also be detected in neutron vibrational spectroscopy in the absence of water in the system.

Finally, the scattering and absorption cross-sections for neutrons are very low so that neutron beams of several cm^2 in area can illuminate samples of several cm^3 because of their high penetration depth. This is in contrast to optical spectroscopies which mainly probe the sample surface and could be a potential problem in our samples, and any hydrogen-bearing minerals in general, because of water concentration gradients and possible partial surface dehydration in opals. The INS has therefore been a preferred method to reliably investigate molecular structures of water in a variety of materials and conditions (*e.g.* Li & Kolesnikov, 2002; Wang & Li, 2003; Kolesnikov *et al.*, 2006; Levy *et al.*, 2009).

It is also important to note that the INS spectra collected on an inverse geometry instrument such as a filter difference spectrometer (FDS) involve an increasing amount of momentum transfer with energy transfer, so that excitations at high energies are significantly broadened in addition to having low intensities because of the small vibrational amplitudes, while optical spectroscopy is done with nearly zero momentum transfer. The high-frequency portion of our vibrational spectra is therefore more informative in the IR than INS data.

Characterization of the samples by X-ray powder diffraction (XRD), Fourier transform infrared spectroscopy (FTIR), transmission electron microscopy (TEM) and neutron diffraction complement the inelastic neutron scattering results.

2. Materials and experimental methods

Three opal samples (opal A1, A2 and C1) formed in sedimentary rocks of Middle to Upper Devonian age at Pedro II, Piaui, northeastern Brazil (Bartoli *et al.*, 1990). One gem opal (opal A3) is from the Finch Claystone facies of the Early Cretaceous Griman Creek Formation from Lightning Ridge, New South Wales, Australia (Watkins, 2000). Opal A1 is faintly translucent with a weak local orange-to-green play of color; opal A2 is less translucent, and more yellow. Opal A3 is green with a green-to-blue play of color. Opal C1 is more uniformly white and milky.

X-ray powder diffraction (XRD) measurements were performed on opals using a PANalytical X'Pert PRO Materials Research Diffractometer at UC Berkeley. Small pieces of opal A1 and C1 were very finely ground and loaded into metal sample holders. The amounts of available opal A2 and A3 were limited. Therefore, small chunks of them were placed on sample holders without grinding. Data were collected using a cobalt target that produces X-rays with a wavelength of 1.789 Å.

Thin slices, 15 μm × 10 μm × 0.15 μm in size, were prepared by a focused ion beam thinning device (FEI FIB200TEM) and analyzed with a FEI Tecnai G2 X-Twin TEM at GeoForschungsZentrum (GFZ) Potsdam, Germany. The instrument is equipped with a Gatan Tridiem energy filter, a Fishione high-angle annular dark-field (HAADF) detector, an EDAX energy dispersive X-ray spectroscopy system (EDS) for chemical characterization, as well as an electron energy loss spectrometer (EELS).

Fourier transform infrared (FTIR) spectra were collected over the mid IR region (500 to 4000 cm^{-1}) at ambient conditions using the KBr pellet procedure with a Thermo-Nicolet Nexus 6700 FTIR spectrometer applying the Attenuated Total Reflectance (ATR) sampling technique at the University of Mainz, Germany. Background spectra were collected under identical conditions before each analysis, spectral resolution was 4 cm^{-1}.

Inelastic neutron scattering (INS) spectra were collected on the FDS at the Manuel Lujan, Jr. Neutron Scattering Center (Taylor *et al.*, 1984). The FDS is an inverse-geometry instrument for inelastic neutron scattering in energy loss with a fixed final energy determined by the bandpass of Be filters placed ahead of the detectors. The energy resolution (ΔE/E) of the instrument can be adjusted in the numerical deconvolution process, and typically ranges from 2–7 % (Hartl *et al.*, 2012), with an energy range from 30 to 6000 cm^{-1}. Data were collected at temperatures of 300 K, 250 K and 10 K. The sample fragments were placed in a sealed cylindrical aluminum sample holder, 5 mm diameter, under a helium atmosphere to avoid water vapor from the air. The sample was analyzed in transmission. The sample holder, heat shield, and vacuum shroud contribute background to the measured

data, which is estimated by collecting a separate spectrum from a vanadium rod, a purely incoherent scatterer. This background spectrum was subtracted from the experimental data using a standard FDS data treatment software (Sivia *et al.*, 1990).

Opal A1 samples for INS measurements consisted of solid pieces with a total mass of 1.9 g. Opal A2 and A3 samples were fragments, 3.9 g and 355 mg, respectively. The opal C1 sample was a single piece with mass of 3.2 g. All samples were cooled from room temperature to 10 K in a closed-cycle refrigerator over a period of approximately 3 hours. Samples — except opal A3 — were subsequently heated to 343 K. The opal A1 and opal C1 samples were also partially dehydrated outside the neutron beam in vacuum for 24 hours at 400 and 720 K. The neutron vibrational spectra of the partially-dehydrated samples were subsequently collected as reference for the identification of vibrational modes of silica-bound hydrogen-containing species.

Neutron powder diffraction data were obtained on fragments of opal A1 with the time-of-flight diffractometers POWGEN (Huq *et al.*, 2011) at SNS and HIPPO (Wenk *et al.*, 2003) at LANSCE. The opal was loaded and sealed in vanadium sample holders in a glove-box under He atmosphere and sealed to avoid contamination from atmospheric water. Measurements were carried out at 290 K and at 100 K. The data presented below are those from the 90° detectors of HIPPO as these have good counting statistics and reasonable resolution. The counting statistics on POWGEN, however, were insufficient to resolve some of the important features in the diffraction patterns because of the much longer flight path, *i.e.* ∼60 m *vs.* ∼9 m on HIPPO and correspondingly a lower flux at the sample position. Counting times on HIPPO were approximately 400 minutes at each temperature. These relatively long counting times ensured that the weak diffraction signal from water could be observed with sufficient accuracy on top of the large incoherent background from the hydrogen atoms in the sample. The neutron diffraction data were processed and analyzed with the software GSAS (Larson & Von Dreele, 2004).

3. Results

3.1. X-ray diffraction

The XRD patterns (Fig. 1), taken at ambient conditions, revealed opal A1, A2 and A3 to be amorphous opal (opal-A) with a single diffuse peak at ∼4.1 Å. Opal C1 shows sharp diffraction peaks at ∼2.5, 4.1 and 4.3 Å and can be classified as opal-CT (Jones & Segnit, 1971). The sharp reflections correspond to low tridymite.

3.2. Transmission electron microscopy

A typical FIB slice of Opal A2 is shown in Fig. 2a. Already on this low-magnification bright-field image a pore

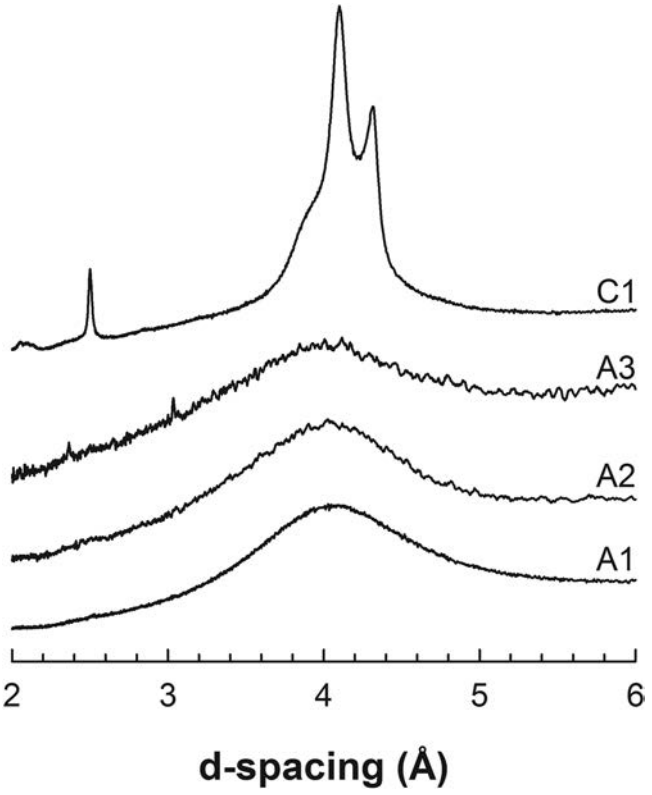

Fig. 1. Powder X-ray diffraction patterns on opal samples reveal that opals A1, A2, A3 are amorphous (opal-A) with a broad diffraction peak at 4 Å, whereas opal C1 is opal-CT (low tridymite).

structure is apparent. The higher magnification image in Fig. 2b shows the spheroidal but cemented particles with some periodicity, visible as linear alignments of pores (white). The average diameter of the spheres is approximately 90 nm; the mean pore space is 50 nm. A Fourier transform of the image in Fig. 2b reveals sharp spots corresponding to the periodic arrangement of amorphous silica spheres in the bright-field image (Fig. 2c).

Opal A1 (Fig. 3) has a similar microstructure as opal A2 (Fig. 2), but the arrangement and size of spherules as well as pores is much more irregular. Pore size is typically 10–20 nm, with occasional larger pores up to 50 nm, illustrated in bright-field (Fig. 3a) and the HAADF-STEM dark-field images (Fig. 3b). A high-resolution image shows a distribution of 0.4 nm distances, but without long-range periodicities (Fig. 3c), which is expressed in the diffuse diffraction ring at 0.4 nm (Fig. 3d).

The most regular arrangement of spherical units is observed in opal A3 (Fig. 4). The spheres are slightly elongated. Also here there are larger and smaller pores but one has to keep in mind that we are looking at 2D sections. The periodic structure displays small pores and large open channels. The periodic stacking is interrupted by ‘‘faults’’ best visible in Fig. 4c.

Opal C1 has an entirely different microstructure with elongated crystallites of tridymite (Fig. 5a). The diffraction pattern displays sharp rings (Fig. 5c), consistent with the XRD results (Fig. 1). Although opal A1, opal A2 and opal

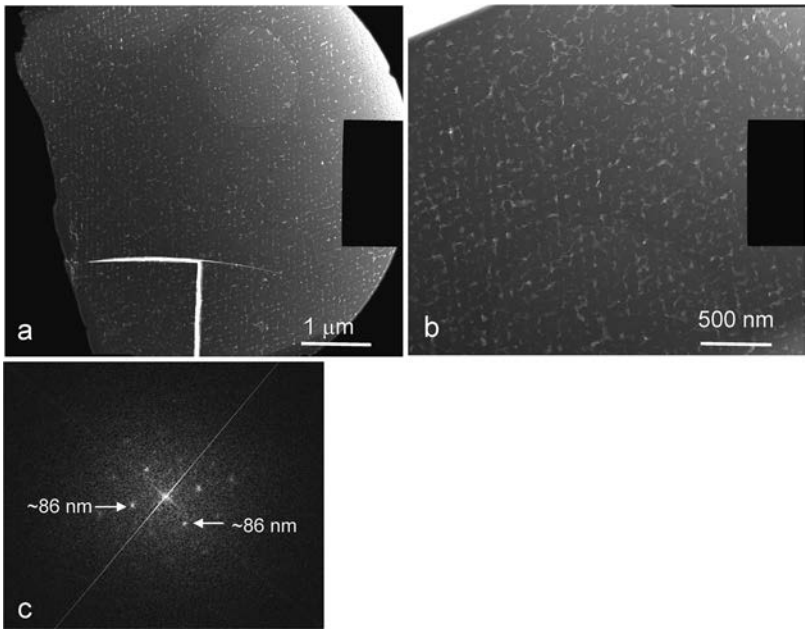

Fig. 2. TEM images of opal A2. (a) Low-magnification bright-field image of FIB slice, (b) bright-field image illustrating regular pore structure, (c) Fourier transform of image in (b) displaying sharp spots at ∼86 nm, indicative of the periodic structure.

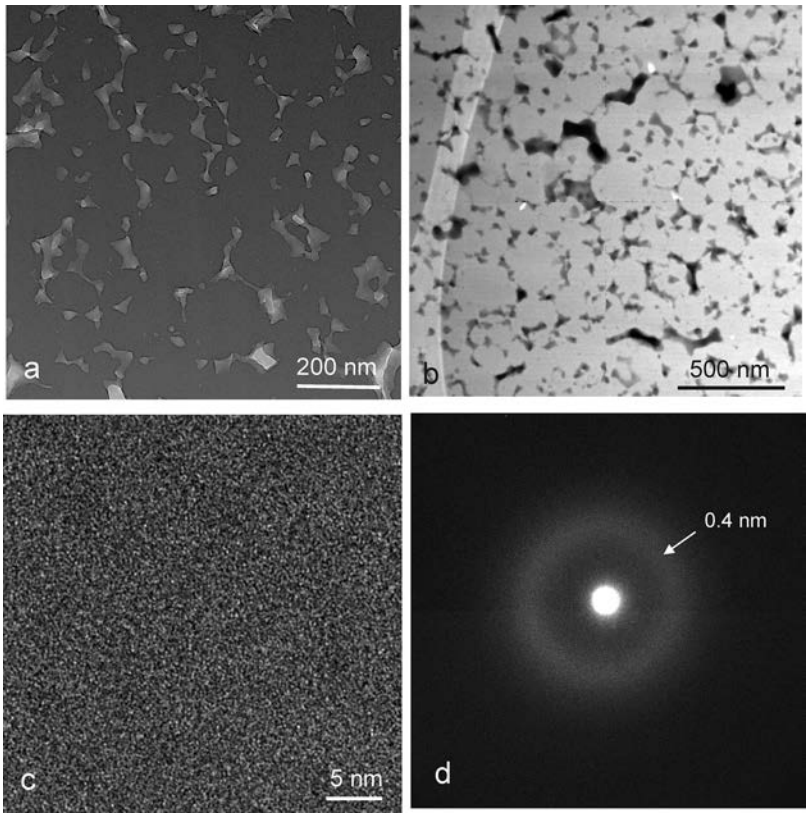

Fig. 3. TEM images of opal A1. (a) Bright-field image, (b) HAADF-STEM image, (c) high-resolution image and (d) selected-area diffraction pattern with a diffuse ring at 0.4 nm (see Fig. 1).

A3 were from the same mine in Brazil and look macroscopically similar, their microstructures are entirely different.

The pore volume has been quantified by segmentation of images, using the software ImageJ (Abramoff *et al.*, 2004). The segmentation is shown in Figs. 4d and 5b. From the 2D

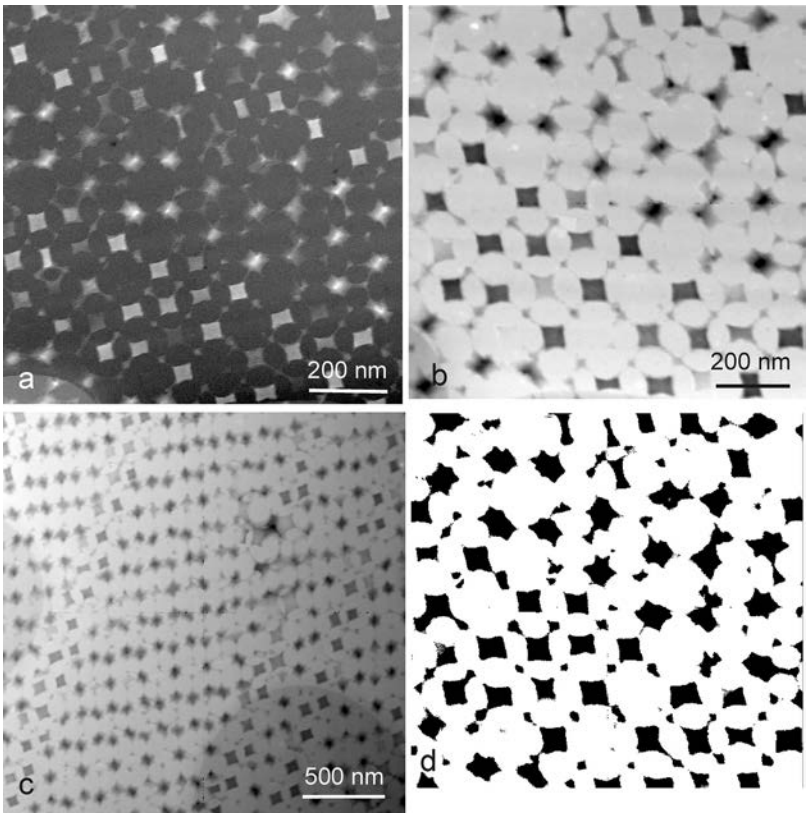

Fig. 4. TEM images of opal A3. (a) Bright-field image, (b,c) HAADF-STEM images (b,c) illustrating regular pore structure. The image (b) has been segmented to calculate the pore volume (d).

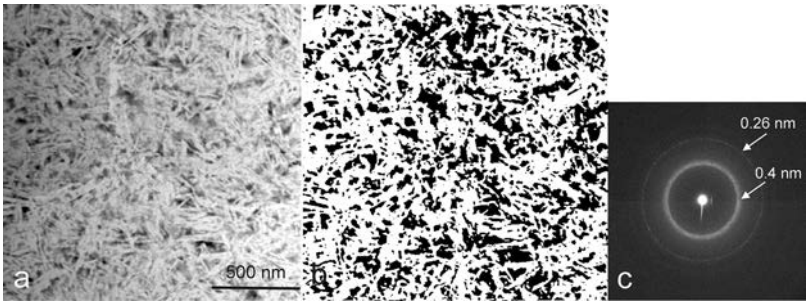

Fig. 5. TEM images of opal C1. (a) HAADF-STEM image of opal CT, (b) segmentation, (c) corresponding diffraction pattern which is consistent with low tridymite (Fig. 1).

segmented images a crude estimation for pore volumes can be made as 24 % for opal A1, 28 % for opal A2, 23 % for opal A3 and 36 % for opal C1. This estimate allows us to conclude that the pore volume of opal CT (opal C1) is larger than that of amorphous opals (A). It should be mentioned that setting segmentation limits in these TEM images is somewhat arbitrary because of the 3D gray contrast through various thicknesses.

3.3. Infrared spectroscopy

The FTIR spectra for the four opal samples obtained from KBr pellets are shown in Fig. 6 to highlight the general characteristics of opal. All IR spectra appear to be very similar to previous studies (*e.g.* Langer & Flörke, 1974; Graetsch *et al.*, 1994; Ilieva *et al.*, 2007; Ostrooumov, 2007; Bobon *et al.*, 2011). The characteristic IR bands for water in opal are found in the area between 1500–4000 cm^{-1} (Fig. 6). We mark on this figure the bands for the H-O-H bending vibration at 1631 cm^{-1} (Aines & Rossman, 1984) and H_2O and the overtone vibration bands at 1880 and 1996 cm^{-1} (Salisbury *et al.*, 1991). The bands at 3410 and 3650 cm^{-1} are related to the O-H stretching modes of hydrogen bonds and of isolated silanol groups, respectively (Langer & Flörke, 1974).

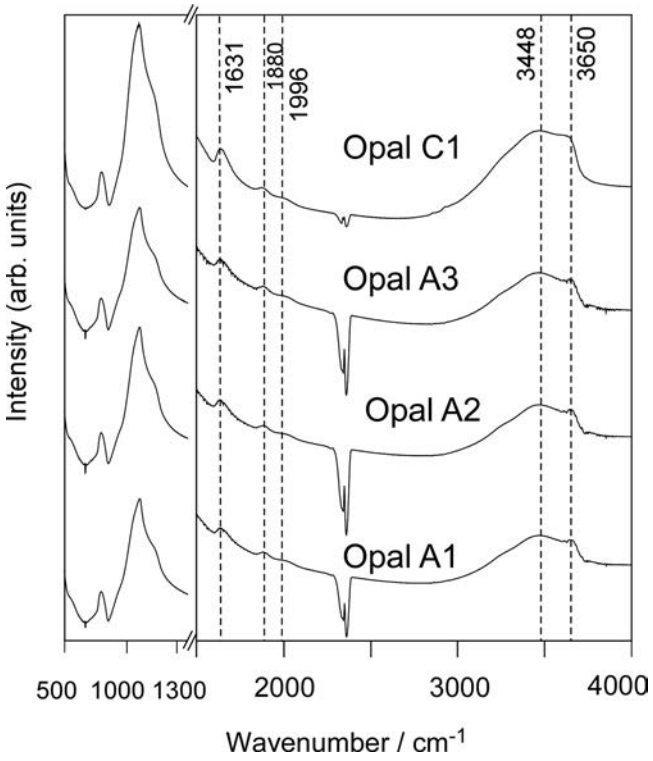

Fig. 6. Measured infrared absorption spectra of the tested opals (spectral resolution 4 cm^{-1}). Marked bands are the H-O-H bending vibration at 1631 cm^{-1} (Aines & Rossman, 1984) and H_2O overtone vibration bands at 1880 and 1996 cm^{-1} (Salisbury *et al.*, 1991). The bands at 3410 and 3650 cm^{-1} are related to the O-H stretching modes of hydrogen bonds and of isolated silanol groups, respectively (Langer & Flörke, 1974). The bands in the region 500–1500 cm^{-1} are mainly related to asymmetric stretching and bending modes of the SiO_4 tetrahedra. The bands at *ca*. 2400 cm^{-1} are the asymmetric stretching modes of CO_2 in air. The water librational modes are contained in the weak feature near 800 cm^{-1}.

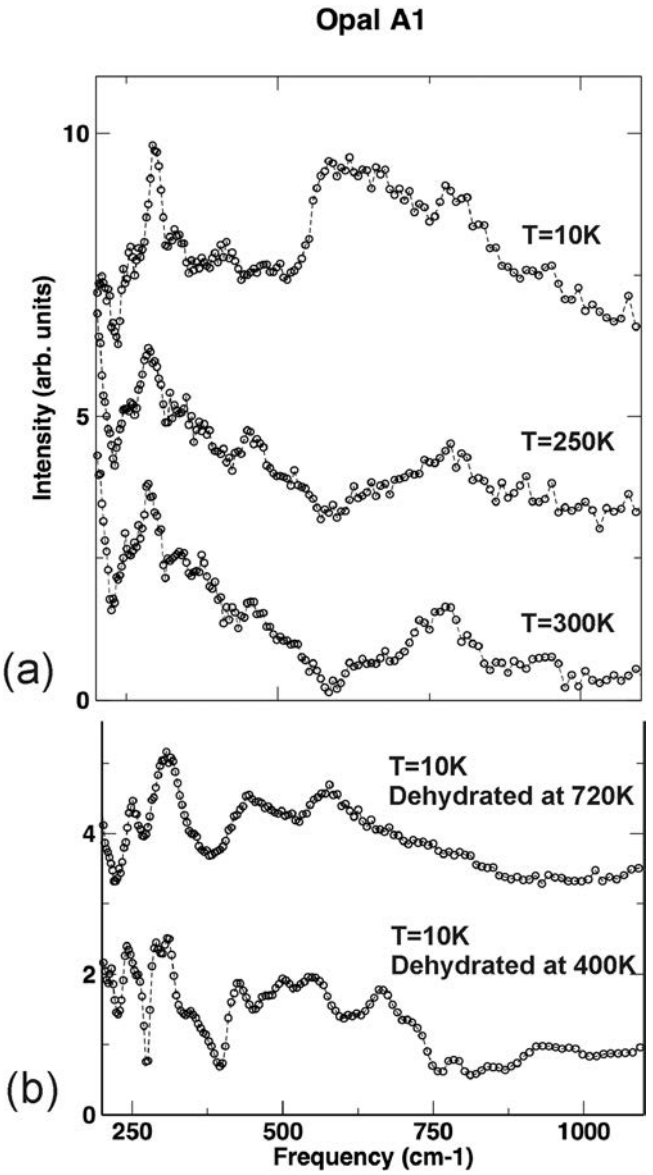

Fig. 7. (a) Background-subtracted inelastic neutron scattering (INS) spectra of opal A1 measured (top to bottom) at 10 K, 250 K and 300 K. (b) Opal A1 dehydrated at 400 K (bottom), 720 K (top); data collected at 10 K.

3.4. Inelastic neutron scattering

The INS vibrational spectra for opal A1 at different temperatures (Fig. 7a) clearly show considerable structure in the librational band (500–1000 cm^{-1}) unlike the corresponding FTIR data (Fig. 6) which look very similar in this range. This band contains the wag, rock and twist of the bound water molecules, which cannot, however, be assigned without computational analysis. The band at approximately 800 cm^{-1}, which persists at high temperatures, may be assigned to a bending mode of silanol groups (see FTIR). Similar spectra were observed at low temperatures in the other opal samples (Fig 8), although they do differ in detail, as will be discussed below. The INS spectra collected at 300 K for three opal A1, A3, and C1 are compared with those obtained at 10 K in Fig. 9, and show a pronounced intensity reduction and/or broadening of in the water librational bands.

Additional experiments were carried out on opal A1 and opal C1. Both samples were heated outside the neutron beam, first to 400 K for 24 hours and then to 720 K for 20 hours in vacuum to first release water and then some of the silanol-associated hydrogen. The INS measurements were repeated after each heating cycle at 10 K. The highly structured librational band in Opal A1 between ~500 to 1100 cm^{-1} is essentially removed (Fig. 7b) after the first heating cycle at 400 K, which clearly indicates that those peaks are due to H_2O. This is emphasized in the difference spectrum (Fig. 10a), which shows that the broad librational band as well as that of the water bending modes (1500–1700 cm^{-1}) are removed by heating to 720 K.

The same experiment was performed for opal C1 (opal-CT sample) with a rather different microstructure (Fig. 10b). We can easily recognize again that the distinct ice-like librational band (Fig. 8, 600–900 cm^{-1}) has completely disappeared after the sample was heated above 400

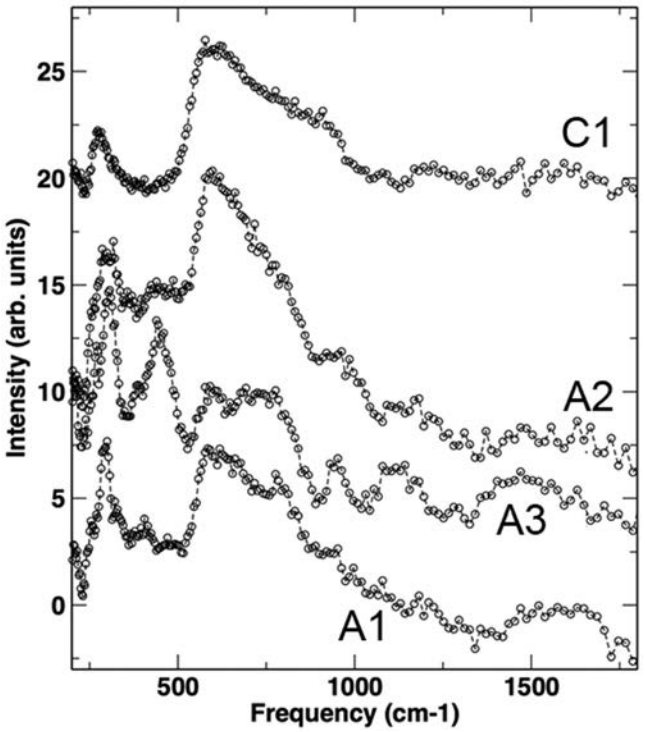

Fig. 8. Inelastic neutron scattering (INS) spectra for four opal samples at 10 K, (top to bottom): C1, A2, A3 and A1.

K. Further heating of either sample to 720 K is expected to remove some of the silanol hydrogens (Fig. 10b), but these spectra are more difficult to interpret as will be discussed below.

3.5. Neutron diffraction

The neutron diffraction data collected at 290 K, 100 K and again at 290 K show distinct occurrence of diffraction peaks at 100 K (Fig. 11). All three datasets show a strong diffuse scattering signal from the amorphous content of the sample, in particular when compared with the data collected for the empty sample container at 100 K. The data for the empty container show only a weak diffraction peak from the thin-walled vanadium can, which also occurs in the opal datasets. The empty sample container was prepared in the same He-filled glove-box as that of the opal sample, to insure similar conditions for both and exclude the possibility that atmospheric water precipitated on the sample container could cause the signal observed at low temperature for the opal. Since the diffuse scattering signal for the opal sample does not change substantially between 290 K and 100 K, we conclude that the strong diffuse scattering in the diffraction pattern is likely due to incoherent scattering of silanols and surface-bound water, along with the amorphous silica (Keen & Dove, 2000), all of which are expected to exhibit only a weak change within the applied temperature range.

The coherent scattering from ice, which results in distinct diffraction peaks at 100 K, can be emphasized by subtracting the 290 K signal from the 100 K signal (Fig. 11; note that this trace is scaled by 10 relative to the other datasets). These data were compared with neutron diffraction patterns for hexagonal and cubic ice generated by GSAS (Larson & Von Dreele, 2004). It is obvious that the opal pattern is consistent with the cubic ice Ic structure (space group *Fd*-3*m*, Shallcross & Carpenter, 1957; Kuhs *et al.*, 1987). In spite of weak intensities, several diffraction peaks can be indexed (Fig. 11) and the lattice parameter for cubic ice in opal at 100 K can be estimated ($a \sim 6.274$ (9) Å). Because of the weak diffraction signals from ice and the limited d-range we could not refine the crystal structure. For comparison the diffraction patterns of ice Ic and ice Ih are also shown (Fig. 11, bottom). Because of the small volume fraction of ice in opal and the high contribution of incoherent scattering, ice Ic diffraction peaks are weak, but nevertheless identifiable. Furthermore opal ice is nanocrystalline, causing a strong decrease of intensity at low d-spacings.

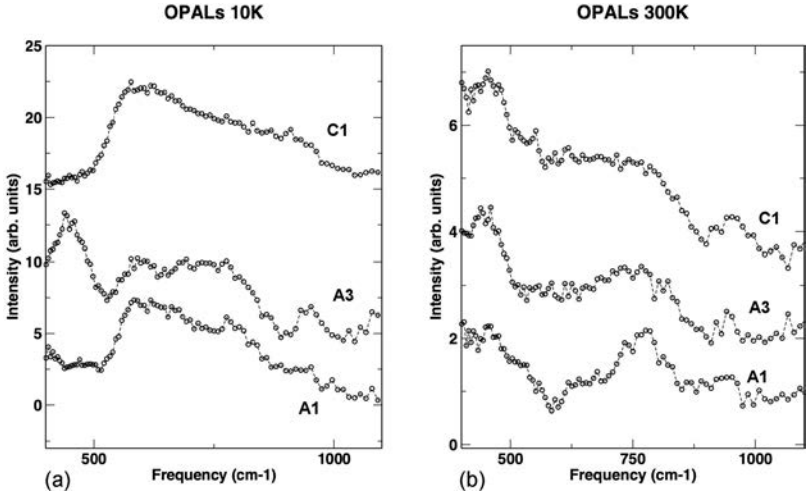

Fig. 9. INS spectra of the water libration region for opals C1, A3 and A1 measured at 10 K (a), and 300 K (b).

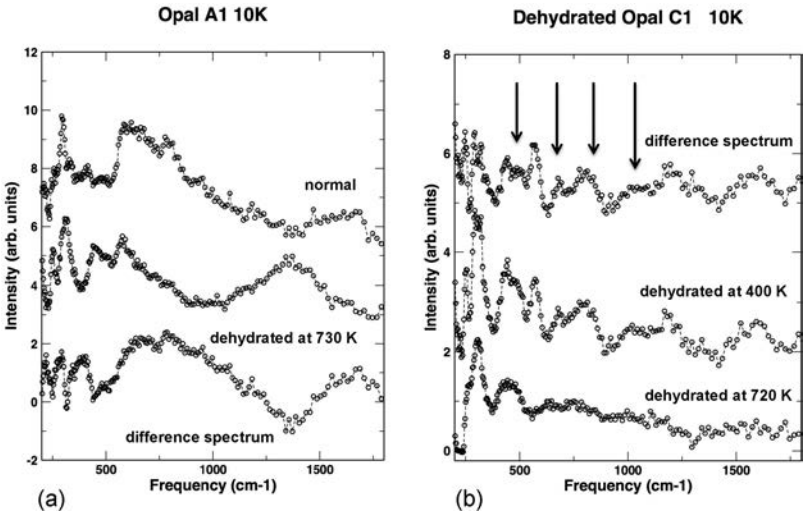

Fig. 10. (a) Removal of interstitial and adsorbed water from Opal A1 upon heating under vacuum to 720 K. The difference spectrum shows the broad water/ice librational band as well as the water bending modes not present in the dehydrated sample. (b) INS spectra of Opal C1 dehydrated at 720 K (bottom), at 400 K (middle) and the difference {400 K–720 K} which emphasizes some of the silanol modes (indicated by arrows).

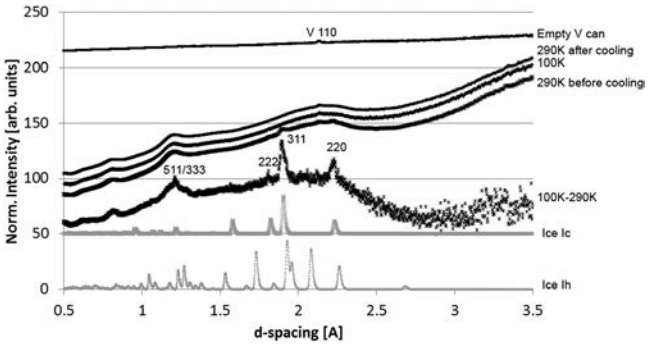

Fig. 11. Neutron diffraction pattern of Opal A1 collected with the TOF HIPPO diffractometer, 90° detector bank. Top: empty vanadium can, below TOF spectra of Opal A1 290 K after cooling, 100 K, 290 K before cooling and below a difference spectrum that displays diffraction peaks of cubic ice (scale 10 times enlarged). For comparison diffraction spectra of ideal cubic and hexagonal ice are shown at the bottom. Intensity scale is arbitrary.

4. Discussion

The four opal samples investigated in this study reveal a wide range of microstructures with varying pore morphologies (Figs. 2–4), yet the FTIR spectra (Fig. 6) do not appear to differ much for the different opals, as for example the H-O-H bending mode at 1631 cm^{-1} (Aines & Rossman, 1984), OH stretching for water at 3448 cm^{-1} and silanols at 3650 cm^{-1} (Dijkstra *et al.*, 2002). The region around the small peak at 700 cm^{-1} in the FTIR spectra (Fig. 6) in turn contains some of the most intense bands in the INS spectra (*e.g.* Fig. 10) for reasons discussed above. The intermolecular librations of H_2O occur in the range from 500 to 1100 cm^{-1} (Denisov *et al.*, 1997; Beta *et al.*, 2004; Eisenberg & Kauzmann, 2005), but their actual positions, shape, and intensity depend strongly on the molecular environment of the water (*e.g.* Tayal *et al.*, 1980), which makes INS a very useful probe for examining the structural and dynamical properties of water within porous systems like opals. In fact, most of the frequency region below 1500 cm^{-1} has received scant attention in optical spectroscopic studies to date because of the weak contributions from water to the optical spectrum and the dominance of the silica scattering,

All investigated opals exhibit a range in pore sizes and many of the smaller pores are not connected by channels. This would mean that when the pores are filled with water, the expansion, which occurs during freezing, may cause locally enhanced pressures. The degree to which this is important in ice formation should also depend on the sizes of the pores. Pore volumes were determined to be 24 % for A1, 28 % for A2, 36 % for C, and 23 % for A3. Inspection of the INS spectra at 10 K for the four Opals (Fig. 8) suggests that the amount of crystalline ice (as represented by the well-defined librational band which starts at about 500 cm^{-1}) scales very roughly with these pore volumes for A1, A2 and C, while A3 with the smallest pore volume exhibits a rather different spectrum with the ice evidently more strongly confined.

The phase diagram of H_2O is very complex with many different polymorphs (*e.g.* Salzmann *et al.*, 2006). In an effort to determine the nature of the ice formed in the pores of the various opals, we can refer to previous INS studies (Li & Kolesnikov, 2002) which report spectra for most phases of ice collected on a similar inverse-geometry spectrometer, TFXA at ISIS, as the FDS at LANSCE. We note, however, that the INS spectra for most of the low-pressures phases are all very similar, for example hexagonal ice Ih, IX, and cubic ice Ic (Figs. 4 and 5, respectively, in Li & Kolesnikov, 2002), which makes phase identification from the INS spectra difficult, if not impossible. In fact, even amorphous ice hda has a similar INS spectrum (Klug *et al.*, 1991). This situation is rather different for many of the

high pressure phases (Fig. 8 in Li & Kolesnikov, 2002), where a pronounced structure in the librational band has been observed for ice II, ice VI and ice VIII. Moreover, the edge of the librational band can shift to lower energies from that in ice Ih.

The latter property may, however, be of some utility in identifying the ice structure formed at low temperature in our opals. Close inspection of the 10 K INS data (Fig. 8) shows that the midpoint of the libration edge for ice in C1 is virtually the same as that for ice Ih (541 cm^{-1}, taken from Fig. 8 in Li & Kolesnikov, 2002), and that the one for ice in opal A1 is in a similar position. The spectra for ice in opals A2 and A3 do have the libration edge at slightly higher frequency (560 cm^{-1}), from which we may conclude that this could well be a structure other than ice Ih, most likely ice Ic. The INS spectrum of ice in opal A1 appears to be an intermediate case, and hence could consist of some ice Ih and Ic.

An accurate identification of the ice structures in the pores of the opals from the INS data would likely require high-level calculations, which would have to include the influence of the surface structure within the pores on ice formation within. Simulations of the vibrational spectra of hexagonal (Ih) and cubic (Ic) ice with Density Functional Theory (DFT) has been described by Morrison (1999) and Casassa *et al.* (2005), using the pseudopotential code AbInit (Gonze *et al.*, 2009). The calculations do not, however, seem to reproduce the actual experimental spectra sufficiently well, and hence may not at this stage be suitable for phase identification.

With increasing temperature the librational edge in the INS spectra softens, the librational bands broaden and become difficult to recognize (Fig. 7a) at 250 K in opal A1. The relatively sharp, ice-like librational band is therefore no longer obvious at 250K (Fig. 7a) and certainly absent at 300 K (Fig. 7a). The peak near 780 cm^{-1} in turn becomes now apparent, and it can readily be assigned to silanol bending modes (Morrow & McFarlan, 1992; Davis & Tomozawa, 1996). Room-temperature INS spectra of Opal C1 and Opal A3 (Fig. 11) show a similar loss of the ice-like librational water spectrum, but we note that the sample with the smallest pore sizes, Opal A3, appears to retain some semblance of a more solid-like water librational spectrum at 300 K.

For opals with larger pores, *i.e*. higher water content, the spectra broaden considerably (Fig. 8) as was also shown for water in zeolites (Jobic *et al.*, 1996). Presumably this may be the result of having water molecules forming widely differing numbers of hydrogen bonds with neighbors, depending on their local, or instantaneous arrangement. This would result in a broad distribution of librational frequencies, which have been shown to depend on the number of H-bonds in a study of water adsorbed on silica gel (Thomas, 1982).

Finally, we briefly discuss the vibrational spectra of the opal samples that were dehydrated under vacuum (Fig. 10). The spectrum after complete dehydration at 720 K resembles that of polycrystalline quartz, in which the broad band at 330 cm^{-1} in amorphous silica is split into two well-defined peaks (Galeener *et al.*, 1983). The difference spectrum (Fig. 10b) with that where the sample was dehydrated at 400 K, consists mainly of the various silanol bands (some of which are indicated by arrows in Fig. 10b), such as bending of different types of single terminal silanols at 800 cm^{-1}, bending modes associated with geminal and bridging silanols (which can occur with the involvement of defects) between 450 cm^{-1} and 550 cm^{-1} (Morrow & McFarlan, 1992; Davis & Tomozawa, 1996; Dijkstra *et al.*, 2002) as well as silica modes which include displacements of the silanol group such as Si-O stretching.

The neutron powder diffraction data from HIPPO supports the presence of cubic ice Ic at 100 K in Opal A1. We note that hexagonal ice Ih (space group $P6_3/mmc$) is not compatible with the indexing of the diffraction peaks as we would expect several more peaks with similar intensities if this form of ice occurred. Apart from the appearance of diffraction peaks at 100 K, a comparison between the 100 K and 290 K data indicates some differences in the diffuse scattering (Fig. 11). These can be attributed to a slight temperature dependence of the diffuse scattering originating from the silica as well as the removal of the comparably weak contribution of water to the diffuse signal due to the solidification of the water at 100 K. There is no evidence for ice O with combined ice Ic and ice Ih stacking which was recently suggested, based on molecular dynamic models (Russo *et al.*, 2014).

Some evidence for the presence of metastable cubic ice has been reported in melted silicate glass (Richet & Polian, 1998), as well as in hydrated glass (Fouzri *et al.*, 2002), and silica nanopores (Dore, 2000; Findenegg *et al.*, 2008; Morishige *et al.*, 2009). Molecular dynamic simulations suggest the presence of ordered Ic in nanopores (Guegan *et al.*, 2005; Moore *et al.*, 2010) and on various surfaces (Feibelman, 2010), thus the presence of Ic in opal is certainly plausible.

5. Conclusions

The existence of a correlation between microstructure and water structure in opals is a novel and important finding. As revealed by INS data there are pronounced differences in the nature of the water content among the various opals at all temperatures. Our exploratory findings deserve to be investigated in greater detail and much more systematically in a wider range of opal structures, in parallel with high-level computational studies. We have clearly shown that vibrational spectroscopy using inelastic neutron scattering in conjunction with neutron powder diffraction provides a powerful tool for investigations of water in opal over the short-range bonding scale.

Acknowledgements: We acknowledge access to FDS and HIPPO at the Lujan Neutron Scattering Center of Los Alamos and POWGEN at SNS. We appreciate help by instrument scientists Luke Daemen (with FDS) and

Ashfia Huq (with POWGEN). The Los Alamos Neutron Science Center and the Spallation Neutron Source are funded by the Department of Energy's Office of Basic Energy Science. This publication was based on work supported in part by Grants from NSF (EAR-1343908) and DOE-BES (DE-FG02-05ER15637). We acknowledge comments from three reviewers that helped us improve the manuscript.

References

Abramoff, M.D., Magelhaes, P.J., Ram, S.J. (2004): Image processing with ImageJ. *Biophot. Inter.*, **11**, 36–42.

Aines, R. & Rossman, G.R. (1984): Water in minerals? A peak in the infrared. *J. Geophys. Res.*, **89**, 4059–4071.

Baier, E. (1932): Die Optik der Edelopale. *Zeitsch. Kristall.*, **81**, 183–218.

Bartoli, F., Bittencourt-Rosa, D., Doirisse, M., Meyer, R., Philippy, R., Samama, J.C. (1990): Role of aluminium in the structure of Brazilian opals. *Eur. J. Mineral.*, **2**, 611–619.

Beta, I.A., Bohlig, H., Hunger, B. (2004): Structure of adsorption complexes of water in zeolites of different types studied by infrared spectroscopy and inelastic neutron scattering. *Phys. Chem. Chem. Phys.*, **6**, 1975–1981.

Bobon, M., Christy, A., Kluvanec, D., Illasova, L. (2011): State of water molecules and silanol groups in opal minerals: a near infrared spectroscopic study of opals from Slovakia. *Phys. Chem. Minerals*, **38**, 809–818.

Brown, L.D., Ray, A.S., Thomas, P.S. (2003): ^{29}Si and ^{27}Al NMR study of amorphous and paracrystalline opals from Australia. *J. Non-Cryst. Solids*, **332**, 242–248.

Casassa, S., Calatayud, M., Doll, K., Minot, C., Pisani, C. (2005): Proton ordered cubic and hexagonal periodic models of ordinary ice. *Chem. Phys. Lett.*, **409**, 110–117.

Davis, K.M. & Tomozawa, M. (1996): An infrared spectroscopic study of water-related species in silica glasses. *J. Non-Cryst. Solids*, **201**, 177–198.

Day, R. & Jones, B. (2008): Variations in water content in Opal-A and Opal-CT from Geyser discharge aprons. *J. Sediment. Res.*, **78**, 301–315.

Denisov, V.P., Venu, K., Peters, J., Hörlein, H.D., Halle, B. (1997): Orientational disorder and entropy of water in protein cavities. *J. Phys. Chem.*, **B 101**, 9380–9389.

Dijkstra, T.W., Duchateau, R., Van Santen, R.A., Meetsma, A., Yap, G.P.A. (2002): Silsesquioxane models for geminal silica surface silanol sites. A spectroscopic investigation of different types of silanols. *J. Am. Chem. Soc.*, **124**, 9856–9864.

Dore, J. (2000): Structural studies of water in confined geometry by neutron diffraction. *Chem. Phys.*, **258**, 327–347.

Eisenberg, D.S. & Kauzmann, W. (2005): The Structure and Properties of Water. Oxford University Press, Oxford, 308pp.

Feibelman, P.J. (2010): The first wetting layer on a solid. *Phys. Today*, **63**, 34–39.

Findenegg, G.H., Jähnert, S., Akcakayiran, D., Schreiber, A. (2008): Freezing and melting of water confined in silica nanopores. *Phys. Chem. Chem. Phys.*, **9**, 2651–2659.

Fouzri, A., Dorbez-Sridi, R., Oumezzine, M. (2002): Water confined in silica gel and in vycor glass at low and room temperature, x-ray diffraction study. *J. Chem. Phys.*, **116**, 791–796.

Gaillou, E., Fritsch, E., Aguilar-Reyes, B., Rondeau, B., Post, J., Barreau, A., Ostroumov, M. (2008): Common gem opal: an investigation of micro- to nano-structure. *Am. Mineral.*, **93**, 1865–1873.

Galeener, F.I., Leadbetter, A.J., Stringfellow, W.M. (1983): Comparison of the neutron, Raman and Infrared vibrational spectra of vitreous SiO_2, GeO_2 and BeF_2. *Phys. Rev.*, **B 27**, 1052–1078.

Gonze, X., Amadon, B., Anglade, P.-M., Beuken, J.-M., Bottin, F., Boulanger, P., Bruneval, F., Caliste, D., Caracas, R., Côté, M. (2009): ABINIT: First-principles approach to material and nanosystem properties. *Comput. Phys. Commun.*, **180**, 2582–2615.

Graetsch, H. & Ibel, K. (1997): Small angle neutron scattering by opals. *Phys. Chem. Minerals*, **24**, 102–108.

Graetsch, H., Gies, H., Topalović, I. (1994): NMR, XRD and IR study on microcrystalline opals. *Phys. Chem. Minerals*, **21**, 166–175.

Guegan, R., Morineau, D., Albasimionesco, C. (2005): Interfacial structure of an H-bonding liquid confined into silica nanopore with surface silanols. *Chem. Phys.*, **317**, 236–244.

Hartl, M., Daemen, L., Muhrer, G. (2012): Water trapped in silica microspheres. *Micropor. Mesopor. Mater.*, **161**, 7–13.

Huq, A., Hodges, J.P., Gourdon, O., Heroux, L. (2011): Powgen: A third-generation high- resolution high-throughput powder diffraction instrument at the Spallation Neutron Source. *Zeitsch. Kristall. Proc.*, **1**, 127–135.

Ilieva, A., Mihailova, B., Tsintsov, Z., Petrov, O. (2007): Structural state of microcrystalline opals: A Raman spectroscopic study. *Am. Mineral.*, **92**, 1325–1333.

Jobic, H., Tuel, A., Krossner, M., Sauer, J. (1996): Water in interaction with acid sites in H-ZSM-5 zeolite does not form hydroxonium ions. A comparison between neutron scattering results and ab initio calculations. *J. Phys. Chem.*, **100**, 19545–19550.

Jones, J.B. & Segnit, E.R. (1971): The nature of opal I. nomenclature and constituent phases. *Aust. J. Earth Sci.*, **18**, 57–68.

Jones, J.B., Sanders, J.V., Segnit, E.R. (1964): Structure of opal. *Nature*, **204**, 990–991.

Kastner, M., Keene, J., Gieskes, J. (1977): Diagenesis of siliceous oozes – I. Chemical controls on the rate of opal-A to opal-CT transformation – an experimental study. *Geochim. Cosmochim. Acta*, **41**, 1041–1059.

Keen, D.A. & Dove, M.T. (2000): Total scattering of silica polymorphs: similarities in glass and disordered crystalline local structure. *Mineral. Mag.*, **64**, 447–457.

Klug, D.D., Whalley, E., Svensson, E.C., Root, J.H., Sears, V.F. (1991): Densities of vibrational states and heat capacities of crystalline and amorphous H_2O ice determined by neutron scattering. *Phys. Rev.*, **B 44**, 841–844.

Kolesnikov, A.I., Li, J.C., Colognesi, D. (2006): Low-energy neutron vibrational spectra of high pressure phases of ice. *Nucl. Instrum. Meth.*, **14**, 325–331.

Kuhs, W.F., Bliss, D.V., Finney, J.L. (1987): High-resolution neutron powder diffraction study of ice Ic. *J. Physique Coll.*, **48**(C-1), 631636.

Langer, K. & Flörke, O.W. (1974): Near infrared absorption spectra (4000–9000 cm^{-1}) of opals and the role of ''water'' in these SiO_2-nH_2O minerals. *Fortsch. Mineral.*, **52**, 17–51.

Larson, A. & Von Dreele, R. (2004): General Structure Analysis System (GSAS). Report LAUR 86–748. Los Alamos National Laboratory, USA.

Levy, E., Kolesnikov, I., Li, J., Mastai, Y. (2009): Structure of water in mesoporous organosilica by calorimetry and inelastic neutron scattering. *Surf. Sci.*, **603**, 71–77.

Li, J.C. & Kolesnikov, A.I. (2002): Neutron spectroscopic investigation of dynamics of water ice. *J. Mol. Liq.*, **100**, 1–39.

Lynne, B.Y. & Campbell, K.A. (2003): Diagenetic transformations (opal-A to quartz) of low-and mid-temperature microbial textures in siliceous hot-spring deposits, Taupo Volcanic Zone, New Zealand. *Can. J. Earth Sci.*, **40**, 1679–1696.

Moore, E.B., de la Llave, E., Welke, K., Scherlis, D.A., Molinero, V. (2010): Freezing, melting and structure of ice in a hydrophilic nanopore. *Phys. Chem. Chem. Phys.*, **12**, 4124–4134.

Morishige, K., Yasunaga, H., Uematsu, H. (2009): Stability of cubic ice in mesopores. *J. Phys. Chem.*, **C 113**, 3056–3061.

Morrison, I. (1999): First principles lattice dynamics studies of the vibrational spectra of ice. *Physica B: Cond. Matt.*, **263–264**, 442–444.

Morrow, B.A. & McFarlan, A.J. (1992): Surface vibrational modes of silanol groups on silica. *J. Phys. Chem.*, **96**, 1395–1400.

Ostrooumov, M. (2007): A Raman, infrared and XRD analysis of the instability in volcanic opals from Mexico. *Spectrochim. Acta*, **A 68**, 1070–1076.

Richet, P. & Polian, A. (1998): Water as a dense icelike component in silicate glasses. *Science*, **281**, 396–398.

Russo, J., Romano, F., Tanaka, H. (2014): New metastable form of ice and its role in the homogeneous crystallization of water. *Nat. Mater.*, **13**, 733–739.

Salisbury, J.W., Walter, L.S., Vergo, N., D'Aria, D.M. (1991): Infrared (2.1–25 Mm) spectra of minerals. Johns Hopkins University Press, Baltimore, MD.

Salzmann, C.G., Radaelli, P.G., Hallbrucker, A., Mayer, E., Finney, J.L. (2006): The preparation and structures of hydrogen ordered phases of ice. *Science*, **311**, 1758–1761.

Shallcross, F.V. & Carpenter, G.B. (1957): X-Ray diffraction study of the cubic phase of ice. *J. Chem. Phys.*, **26**, 782–784.

Sivia, D.S., Vorderwisch, P., Silver, R.N. (1990): Deconvolution of data from the filter difference spectrometer: from hardware to maximum entropy. *Nuc. Instrum. Meth. Phys. Res.*, **290**, 492–498.

Sosnowska, I., Buchenau, U., Reichenauer, G., Graetsch, H., Ibel, K., Frick, B. (1997): Structure and dynamics of the opal silica-water system. *Physica B*, **234–236**, 455–457.

Tayal, V.P., Srivastava, B.K., Khandelwal, D.P., Bist, H.D. (1980): Librational modes of crystal water in hydrated solids. *Appl. Spectrosc. Rev.*, **16**, 43–134.

Taylor, A., Wood, E., Goldstone, J., Eckert, J. (1984): Lineshape analysis and filter difference method for a high intensity time-of-flight inelastic neutron scattering spectrometer. *Nuc. Instrum. Meth. Phys. Res.*, **221**, 408–418.

Thomas, R.K. (1982): Neutron scattering from adsorbed systems. *Prog. Solid State Chem.*, **14**, 1–93.

Wang, Y. & Li, J.C. (2003): Diffuse neutron-scattering studies of ice Ih under high pressures. *Can. J. Phys.*, **81**, 409–413.

Watkins, J.J. (2000): The Opal Bug. *New South Wales Department of Mineral Resources Minfo*, **65**, 26–29.

Wenk, H.-R., Lutterotti, L., Vogel, S. (2003): Texture analysis with the new HIPPO TOF diffractometer. *Nuc. Instrum. Meth.*, **A 515**, 575–588.

Received 17 March 2014
Modified version received 1 December 2014
Accepted 2 December 2014